Quantitative dynamic force microscopy with inclined tip oscillation

Philipp Rahe[*], Daniel Heile, Reinhard Olbrich and Michael Reichling

Abstract

In the mathematical description of dynamic atomic force microscopy (AFM), the relation between the tip–surface normal interaction force, the measurement observables, and the probe excitation parameters is defined by an average of the normal force along the sampling path over the oscillation cycle. Usually, it is tacitly assumed that tip oscillation and force data recording follows the same path perpendicular to the surface. Experimentally, however, the sampling path representing the tip oscillating trajectory is often inclined with respect to the surface normal and the data recording path. Here, we extend the mathematical description of dynamic AFM to include the case of an inclined sampling path. We find that the inclination of the tip movement can have critical consequences for data interpretation, especially for measurements on nanostructured surfaces exhibiting significant lateral force components. Inclination effects are illustrated by simulation results that resemble the representative experimental conditions of measuring a heterogeneous atomic surface. We propose to measure the AFM observables along a path parallel to the oscillation direction in order to reliably recover the force along this direction.

Introduction

Atomic force microscopy (AFM) is a quantitative technique that allows for probing the force field above a surface in one, two, or three dimensions. While imaging in a plane parallel to the surface provides nanoscale and atomic structural information [1], force curves, usually acquired along a recording path perpendicular to the surface, provide quantitative information about the details of the tip–surface interaction when properly analysed [2]. Recently, a universal description of quantitative

dynamic force microscopy based on the harmonic approximation has been developed [3], yielding three central equations that link the physical interaction parameters force $\vec{F}_{ts}$ and damping $\vec{\gamma}_{ts}$ with the measurement observables static deflection q_s, oscillation amplitude A, and phase φ as well as the excitation parameters frequency f_{exc} and force F_{exc}. This theory specifically predicts the distant-dependent frequency shift of a tip moved perpendicular to a surface for a given force curve.

Inversion formulae are available that allow for the extraction of the interaction force from measured frequency-shift data [4,5].

A tacit assumption of all prevalent algorithms for force inversion is that the axis of data acquisition (herein denoted as the recording path, usually the axis of the piezo scanner, z_p) is parallel to the axis of the oscillation (herein denoted as the sampling path). However, in a typical experimental setup this is not the case. Instead, angles of 10° to 20° between these two directions are often present for technical reasons. Consequences of this inclined AFM cantilever mount have been identified before, in particular for atomic force microscopy performed in static ("contact") mode where an effective spring constant [6-8] has been introduced and a torque [9,10] as well as load [11] correction has been applied. Additionally, a tilted cantilever has been found to lead to a modification of the tip–sample convolution [12], to enhance the sensitivity of the measurement to the probe side [13], and to influence results of multifrequency AFM and Kelvin probe force microscopy [14]. In the presence of a viscous damping layer, in-plane dissipation mechanisms have been found to cause systematic changes of the phase shift in amplitude-modulation AFM depending on the cantilever inclination [15]. Furthermore, it has been proposed to use the presence of a lateral component in the tip oscillation path for the investigation of in-plane material properties, such as the in-plane shear modulus [16]. Last, the influence of the inclination between oscillation direction and surface plane has been used in lateral force microscopy to determine the probe oscillation amplitude [17].

Here, we extend the established mathematical description for dynamic atomic force microscopy [3] by including free orientations of the tip sampling and data recording paths. The resulting formulae are discussed and implications for precise force measurements [2] are identified and quantified. Most importantly, the data acquisition with an inclined tip sampling path requires modifications of the experimental procedures and data analysis protocols for force measurements to avoid systematic errors in the interpretation of force curve and imaging data.

Results and Discussion
Sensor positioning, sensor displacement, and tip position
Prerequisite to quantitative force microscopy is a precise definition of the involved probe and sample coordinates as well as probe dynamical parameters that are outlined in the following.

In dynamic AFM, the force $\vec{F}_{ts}$ acting between a sharp tip and the surface under investigation is measured as a function of the tip position $\vec{r}_{ts}$ that is usually described in Cartesian coordinates with the origin placed in the sample surface and the z-axis with unit vector $\vec{e}_z$ oriented perpendicular to the surface as shown in Figure 1. Lateral movements of the tip as applied for imaging are associated with the x and y axes, while the tip–surface distance z_{ts} is measured along the z-axis. In most AFM implementations, the force measurement is restricted to nominally measuring the normal component of the tip–sample force $F_{ts}^z = \vec{F}_{ts} \cdot \vec{e}_z$, often denoted by F_N. The ideal force curve
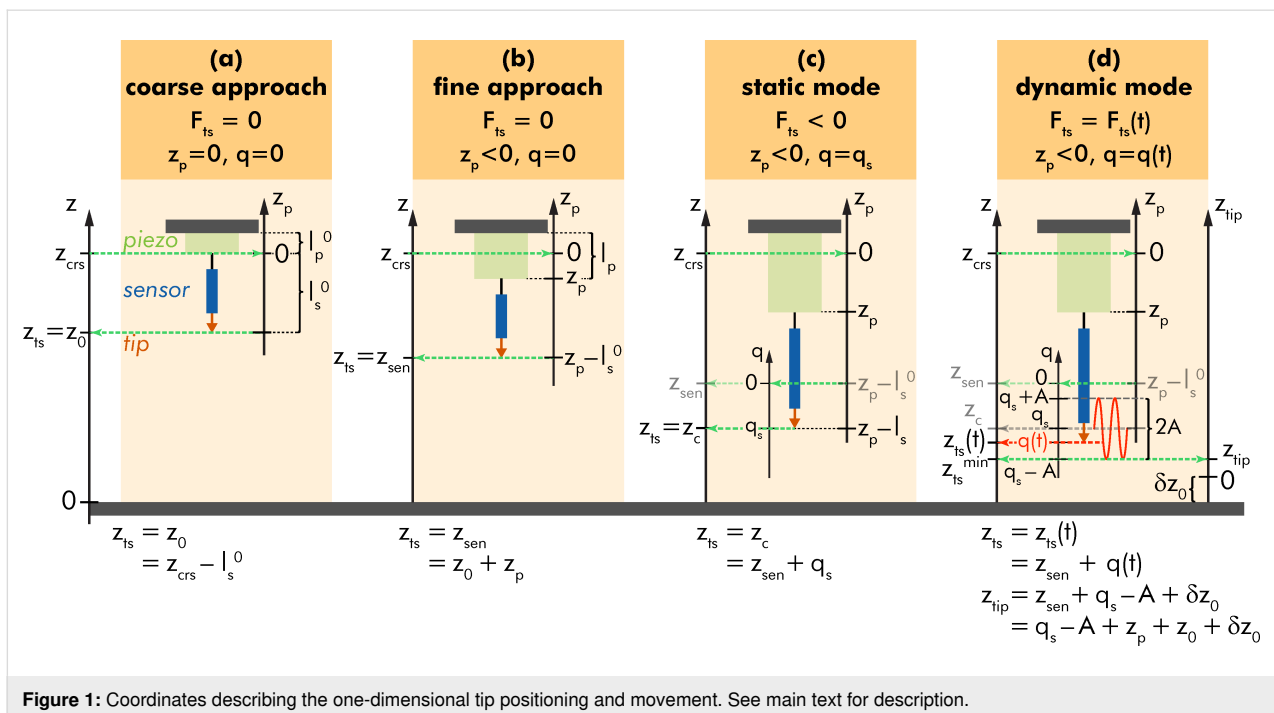
Figure 1: Coordinates describing the one-dimensional tip positioning and movement. See main text for description.

is a measurement of $F_{ts}^z(z_{ts})$ while the measurement of $F_{ts}^z(x_{ts}, y_{ts}, z_{ts})$ is referred to as force mapping.

To measure the tip–surface force in a dynamic measurement, the force probe acts as a high-Q oscillator and elastically responds to $\vec{F}_{ts}$ by static and dynamic displacement described by $q = \vec{q} \cdot \vec{e}_q$ with $\vec{e}_q$ being the unit vector along the tip sampling path. This path is usually straight and assumed to be strictly parallel to $\vec{e}_z$. Furthermore, we assume an infinitely stiff sensor in directions perpendicular to $\vec{e}_q$ as well as a linear sensor response along $\vec{e}_q$. Then, the static probe response follows Hooke's law $F_{ts}^z(x_{ts}, y_{ts}, z_{ts}) = kq$, with k being the static sensor force constant [18]. In dynamic mode operation, the sensor is excited to periodic displacement $q(t) = q(t + 1/f_{exc})$ along the q-axis at an excitation frequency f_{exc}.

To bring the tip in the desired range of interaction with the surface and to perform the movements required for imaging, force mapping, and taking force curves, the sensor is moved by coarse and fine positioning elements acting at least along the z-axis. To accomplish this, the sensor is attached to a piezo element allowing for fine positioning that, in turn, is attached to a coarse positioning system. The respective sensor positioning movements, the sensor oscillation, and its response to the mean tip–surface force are illustrated in the sketches of Figure 1 for the case of parallel tip sampling and data recording paths.

Initially, the sensor assembly is moved towards the surface by the coarse positioning system so that the relaxed piezo rests at position z_{crs} and the tip at its starting position z_0 (Figure 1a). In its relaxed state, the z piezo and the force sensor have a length of l_p^0 and l_s^0, respectively. Applying a voltage to the z-piezo results in an extension of the piezo length l_p that is described as a piezo position z_p on the separate axis z_p with unit vector $\vec{e}_p$ and with the origin chosen to coincide with the z_{crs} position (Figure 1b). As the unit vectors $\vec{e}_z$ and $\vec{e}_p$ are chosen to point into the same direction, a piezo extension $z_p < 0$ results in an approach of the tip towards the surface while $z_p > 0$ indicates a tip retraction. Coarse and fine approach define the sensor position $z_{sen} = z_0 + z_p$, which is at this point identical to the tip position (tip–sample distance) z_{ts} as the force F_{ts} acting on the tip is unmeasurably small for sufficiently large z_{ts}. Upon further approach of the sensor, however, the tip experiences a measureable force, yielding a static sensor displacement q_s described on the q-axis with the origin chosen at z_{sen}, corresponding to the tip centre position $z_c = z_{sen} + q_s$ (Figure 1c). As $\vec{e}_z$ and $\vec{e}_q$ point in the same direction, a sensor displacement $q < 0$ corresponds to a tip movement towards the surface. Note that the tip centre position z_c cannot easily be set or determined as the static sensor displacement is governed by the a priori unknown force curve. Furthermore, q_s is usually so small that it is at or beyond the

limit of detectability for most NC-AFM implementations. In dynamic NC-AFM operation, the sensor oscillates with an amplitude A symmetrical to the static displacement q_s with turning points $q_s + A$ and $q_s - A$ (Figure 1d). The momentary tip position at time t can either be described as the displacement $q(t)$ or as the position $z_{ts}(t)$, whereby the lower turning point z_{ts}^{min} is the point of strongest tip–surface interaction.

While the tip position and sensor dynamics can principally be well described by the respective positions on the z-axis, this axis is practically of limited use as its zero point cannot be defined or determined in a reasonable way. This is due to the fact that neither z_{crs} nor l_s^0 can be determined with atomic-scale precision, which would be needed for properly taking into account the force curve $F_{ts}^z(z_{ts})$. Furthermore, it is conceptually difficult to define the position of the surface at the atomic scale. As every force curve acquired on a surface diverges for $z_{ts} \to 0$, the natural choice of the z-axis origin would be the z value approached by the diverging force. This point is, however, experimentally not accessible. Instead, precise values for the piezo position z_p and the sensor displacement $q(t)$ are experimentally available. To derive a force–distance curve experimentally, the usual procedure is therefore to apply dynamic AFM and to measure the distance-dependent shift in frequency, $\Delta f(z_p)$, of the sensor excitation frequency f_{exc} that results when phase resonance for the sensor oscillation is maintained throughout the measurement [19]. The resulting curve $\Delta f(z_p)$ is a convolution of the covered part of the force curve $F_{ts}^z(z_{ts})$ and a kernel depending on the stabilised sensor oscillation amplitude A. A sophisticated analysis of the $\Delta f(z_p)$ curves measured with different oscillation amplitudes A yields a precise result [2] for the force curve, yet with an arbitrary origin along the z-axis. In theoretical modelling and analysis of tip–sample interactions, it has been established as a standard to represent force curves as $F_{ts}^z = F_{ts}^z(z_{ts}^{min})$ [4,5]. As z_{ts}^{min} is practically not accessible, for the representation of force curves we introduce an axis z_{tip} that is identical to the z-axis except for an unknown offset δz_0 for the tip starting position and describe a force curve resulting from the analysis of measured data as $F_{ts}^z(z_{tip})$ where $z_{tip} = z_{ts}^{min} - \delta z_0$.

Geometry for the inclined sampling path

A tip sampling path inclined relative to the z-axis implies that the direction of oscillation $\vec{e}_q$ is tilted with respect to $\vec{e}_z$ as illustrated in Figure 2. We introduce the inclined axis w parallel to the tip sampling path with $\vec{e}_w$ pointing in the direction of $\vec{e}_q$. Assuming an inclination angle of α (with $0 \leq \alpha \leq \pi/2$) between $\vec{e}_z$ and $\vec{e}_q$, any position on the w-axis can be expressed by the respective position on the z_{tip}-axis by a simple geometrical transformation. This implies that any sensor movement along z_p is not in line with the tip sampling path. Therefore, one has to

take into account that the inclined oscillatory motion of the sensor can invoke significant lateral movement of the tip when describing the Δf signal formation and force deconvolution. If the force field $\vec{F}_{ts}\left(\vec{r}_{ts}\right) = \vec{F}_{ts}\left(x_{ts}, y_{ts}, z_{ts}\right)$ above the surface is homogeneous and isotropic with respect to the lateral coordinates x_{ts} and y_{ts}, the inclined axis of sensor oscillation can be taken into account by using transformed position variables $z_p \rightarrow z_p \cos\alpha$ or $z_{tip} \rightarrow z_{tip} \cos\alpha$.
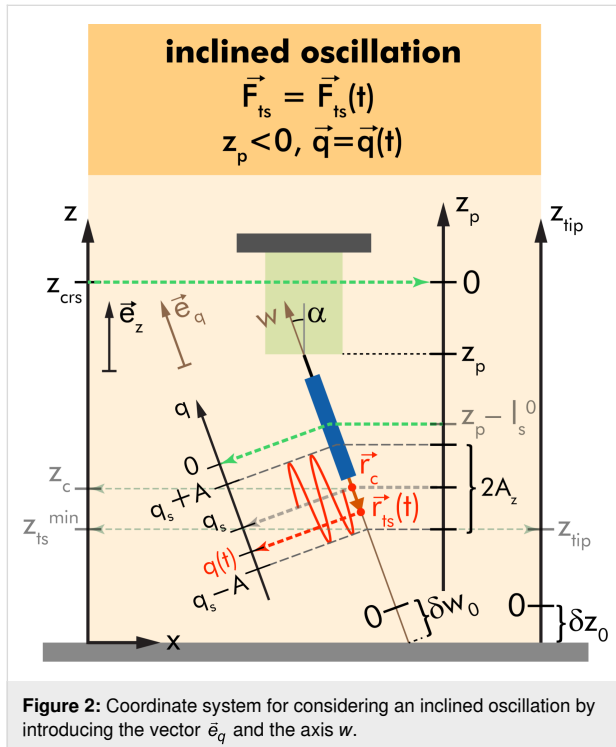

Figure 2: Coordinate system for considering an inclined oscillation by introducing the vector $\vec{e}_q$ and the axis w.

If no such homogeneity is present, however, the w-axis has to be taken explicitly into account. The definition of a zero position of this w-axis goes along the same lines as the definition of zero δz_0 for the z_{tip}-axis by introducing w_{ts}^{min} and the uncertainty δw_0.

For the further discussion, we define the vectorial sensor displacement $\vec{q}$ as

$$\vec{q}\left(t\right) = q\left(t\right) \cdot \vec{e}_q. \tag{1}$$

Within the harmonic approximation [3], $q(t)$ is given as

$$q\left(t\right) = q_s + A \cdot \cos\left(2\pi f_{exc} t + \varphi\right) \tag{2}$$

with the static deflection q_s, the oscillation amplitude A, the excitation frequency f_{exc}, and the phase φ [3]. In its vectorial

form, the momentary position of the tip $\vec{r}_{ts}\left(t\right)$ is given as

$$\vec{r}_{ts}\left(t\right) = \vec{r}_0 + \vec{r}_p + \vec{q}\left(t\right) \tag{3}$$

$$= \vec{r}_c + A \cdot \cos\left(2\pi f_{exc} t + \varphi\right) \cdot \vec{e}_q \tag{4}$$

with the centre position $\vec{r}_c = \vec{r}_0 + \vec{r}_p + q_s \vec{e}_q$, start position $\vec{r}_0$, and piezo position $\vec{r}_p$. These quantities generalise the previously introduced z coordinates z_c, z_0, and z_p, respectively. We further introduce the reduced amplitude A_z as the projection of A on the surface normal [2]

$$A_z = A \cdot \cos\alpha. \tag{5}$$

Equation of motion for the inclined sampling path

Next, we derive the three AFM equations [3] linking the AFM physical parameters with the experimental observables and excitation parameters for a straight tip sampling path with arbitrary oscillation direction. The starting point is the differential equation describing the displacement $q(t)$ in presence of the tip–sample force field $\vec{F}_{ts}\left(\vec{r}_{ts}, \dot{\vec{r}}_{ts}\right)$ and excitation force F_{exc}^q as follows

$$0 = -\frac{k_0}{\left(2\pi f_0\right)^2}\ddot{q} - k_0 q - \frac{k_0}{2\pi f_0 Q_0}\dot{q} + F_{exc}^q\left(t\right) + F_{ts}^q\left(q, \dot{q}\right) \tag{6}$$

with the sensor parameters fundamental eigenfrequency f_0, modal sensor stiffness k_0 [18], and modal sensor quality factor Q_0. This equation of motion is a one-dimensional differential equation depending on the tip–sample force component $F_{ts}^q = \vec{F}_{ts}\left(\vec{r}_{ts}, \dot{\vec{r}}_{ts}\right) \cdot \vec{e}_q$, following the description in [3,15,16]. The vectorial tip–sample force can generally be expressed by the sum of an even, $\vec{F}_{even}$, and an odd, $\vec{F}_{odd}$, component

$$F_{ts}^q = \vec{F}_{even} \cdot \vec{e}_q + \vec{F}_{odd} \cdot \vec{e}_q. \tag{7}$$

The deflection q is periodic with $T_{exc} = f_{exc}^{-1}$ and the tip–sample force component F_{ts}^q can, therefore, be expressed by the Fourier sum

$$F_{ts}^q = F_{even}^{q,0}$$
$$+ \sum_{n=1}^{\infty}\left[F_{even}^{q,n}\cos\left(2\pi f_{exc} t + \varphi\right) + F_{odd}^{q,n}\sin\left(2\pi f_{exc} t + \varphi\right)\right] \tag{8}$$

with the coefficient for $n = 0$

$$F_{\text{even}}^{\text{q},0} = f_{\text{exc}} \int_0^{T_{\text{exc}}} \vec{F}_{\text{even}}\left(\vec{r}_{\text{ts}}(t), \dot{\vec{r}}_{\text{ts}}(t)\right) \cdot \vec{e}_q \, \mathrm{d}t \qquad (9)$$

and the coefficients for $n \geq 1$

$$F_{\text{even}}^{\text{q},n} = 2 f_{\text{exc}} \int_0^{T_{\text{exc}}} \vec{F}_{\text{ts}}\left(\vec{r}_{\text{ts}}(t), \dot{\vec{r}}_{\text{ts}}(t)\right) \cdot \vec{e}_q \cos\left(2\pi n f_{\text{exc}} t + \varphi\right) \mathrm{d}t \quad (10)$$

$$F_{\text{odd}}^{\text{q},n} = 2 f_{\text{exc}} \int_0^{T_{\text{exc}}} \vec{F}_{\text{ts}}\left(\vec{r}_{\text{ts}}(t), \dot{\vec{r}}_{\text{ts}}(t)\right) \cdot \vec{e}_q \sin\left(2\pi n f_{\text{exc}} t + \varphi\right) \mathrm{d}t. \quad (11)$$

With the time average defined by [3]

$$\left\langle \vec{f} \cdot \vec{e}_q \right\rangle_t = \left\langle f^q \right\rangle_t = f_{\text{exc}} \int_0^{T_{\text{exc}}} f^q(t) \mathrm{d}t = f_{\text{exc}} \int_0^{T_{\text{exc}}} \vec{f}(t) \cdot \vec{e}_q \, \mathrm{d}t, \quad (12)$$

for an arbitrary function $\vec{f}$ with projection $f^q = \vec{f} \cdot \vec{e}_q$, the Fourier coefficients for $n \geq 1$ can be expressed in terms of time averages

$$F_{\text{even}}^{\text{q},0} = \left\langle \vec{F}_{\text{even}} \cdot \vec{e}_q \right\rangle_t = \left\langle F_{\text{even}}^q \right\rangle_t \qquad (13)$$

$$F_{\text{even}}^{\text{q},n} = 2 \left\langle \vec{F}_{\text{ts}} \cdot \vec{e}_q \cos\left(2\pi n f_{\text{exc}} t + \varphi\right) \right\rangle_t \qquad (14)$$

$$F_{\text{odd}}^{\text{q},n} = 2 \left\langle \vec{F}_{\text{ts}} \cdot \vec{e}_q \sin\left(2\pi n f_{\text{exc}} t + \varphi\right) \right\rangle_t. \qquad (15)$$

AFM equations for the inclined sampling path

The three AFM equations follow from evaluating the Fourier coefficients $F_{\text{even}}^{\text{q},0}$, $F_{\text{even}}^{\text{q},1}$, and $F_{\text{odd}}^{\text{q},1}$. The first step is to calculate the time-averaged form of the three equations (see Appendix section for the derivations)

$$\left\langle \vec{F}_{\text{even}} \cdot \vec{e}_q \right\rangle_t = k_0 q_s \qquad (16)$$

$$\left\langle \vec{F}_{\text{even}} \cdot \vec{e}_q (q - q_s) \right\rangle_t = \frac{k_0 A^2}{2}\left(1 - \frac{f_{\text{exc}}^2}{f_0^2}\right) - \frac{A F_{\text{exc}}^q}{2} \cos\varphi \quad (17)$$

$$\left\langle \vec{F}_{\text{odd}} \cdot \vec{e}_q \dot{q} \right\rangle_t = \frac{\pi k_0 A^2 f_{\text{exc}}^2}{f_0 Q_0} + \pi f_{\text{exc}} A F_{\text{exc}}^q \sin\varphi. \qquad (18)$$

In a next step, the time averages are transformed to spatial averages similar to the formerly introduced cup and cap average functionals [3].

The harmonic approximation constrains the tip movement within the $\left(\vec{r}_{\text{ts}}, \dot{\vec{r}}_{\text{ts}}\right)$ phase space to a closed trajectory. Consequently, the parametrisation with a spatial coordinate along this sampling path requires a parametrisation of the velocity by this coordinate as well. To reflect this dependency, we introduce the even force $\vec{F}_{\text{even}}^\circ(\vec{r}_{\text{ts}})$, formally defined by $\vec{F}_{\text{even}}^\circ(\vec{r}_{\text{ts}}) = \vec{F}_{\text{even}}\left(\vec{r}_{\text{ts}}, \dot{\vec{r}}_{\text{ts}}(\vec{r}_{\text{ts}})\right)$ as the force along the tip sampling path. Then, we further define the projection of an arbitrary function $\vec{f}^\circ$ along the tip sampling path on the oscillation direction $\vec{e}_q$ as $f^{\circ q} = \vec{f}^\circ \cdot \vec{e}_q$ and perform the integration along the sampling path symmetrically to the centre position $\vec{r}_{\text{c}}$ of this projected quantity $f^{\circ q}$. The cup and cap averaging functionals are then written as

$$\left\langle \vec{f}^\circ \cdot \vec{e}_q \right\rangle_\cup (\vec{r}_{\text{c}}) = \left\langle f^{\circ q} \right\rangle_\cup (\vec{r}_{\text{c}})$$
$$= \int_{-A}^{A} \vec{f}^\circ(\vec{r}_{\text{c}} + q'\vec{e}_q) \cdot \vec{e}_q \frac{1}{\pi\sqrt{A^2 - (q')^2}} \mathrm{d}q' \qquad (19)$$

$$\left\langle \vec{f}^\circ \cdot \vec{e}_q \right\rangle_\cap (\vec{r}_{\text{c}}) = \left\langle f^{\circ q} \right\rangle_\cap (\vec{r}_{\text{c}})$$
$$= \int_{-A}^{A} \vec{f}^\circ(\vec{r}_{\text{c}} + q'\vec{e}_q) \cdot \vec{e}_q \frac{2}{\pi A^2}\sqrt{A^2 - (q')^2} \mathrm{d}q'. \qquad (20)$$

These averages have now the structure of line integrals along the tip sampling path parallel to $\vec{e}_q$, spanning the range $-A$ to A as parameterised by q'.

We furthermore define the tip–sample force gradient along the oscillation path, $\bar{k}_{\text{ts}}^\circ$, by the derivation of the force along the oscillation direction, namely

$$\bar{k}_{\text{ts}}^\circ(\vec{r}_{\text{c}} + q'\vec{e}_q) = \frac{\mathrm{d}}{\mathrm{d}q'}\vec{F}_{\text{even}}^\circ(\vec{r}_{\text{c}} + q'\vec{e}_q). \qquad (21)$$

The three AFM equations follow now from Equation 16, Equation 17, and Equation 18 as

$$\left\langle \vec{F}_{\text{even}}^\circ \cdot \vec{e}_q \right\rangle_\cup (\vec{r}_{\text{c}}) = k_0 q_s. \qquad (22)$$

$$\left\langle \bar{k}_{\text{ts}}^\circ \cdot \vec{e}_q \right\rangle_\cap (\vec{r}_{\text{c}}) = k_0\left(1 - \frac{f_{\text{exc}}^2}{f_0^2}\right) - \frac{F_{\text{exc}}^q}{A}\cos\varphi \qquad (23)$$

$$\left\langle \vec{\gamma}_{\text{ts}}^{\circ} \cdot \vec{e}_q \right\rangle_{\cap} (\vec{r}_{\text{c}}) = -\frac{k_0}{2\pi Q_0 f_0} - \frac{F_{\text{exc}}^q}{2\pi f_{\text{exc}} A} \sin \varphi \qquad (24)$$

whereby the vectorial damping coefficient $\vec{\gamma}_{\text{ts}}$ and the damping coefficient $\vec{\gamma}_{\text{ts}}^{\circ}$ along the oscillation path have been introduced to write the odd force as

$$\vec{F}_{\text{odd}} \left(\vec{r}_{\text{ts}}, \dot{\vec{r}}_{\text{ts}} \right) = -\vec{\gamma}_{\text{ts}} \left(\vec{r}_{\text{ts}}, \dot{\vec{r}}_{\text{ts}} \right) \cdot \dot{q} = \vec{\gamma}_{\text{ts}}^{\circ} (\vec{r}_{\text{ts}}) \cdot \dot{q}. \qquad (25)$$

Force response for the inclined sampling path

By reinterpreting the cup and cap averaging functionals as line integrals along the inclined tip sampling path, three AFM equations were found that represent the general case for a probe oscillating in an arbitrary direction. A probe orientation different from the surface normal and its oscillation in the vector force field above the surface has important consequences on the measured force response and appropriate data analysis procedures.

We demonstrate these consequences by simulating the frequency shift $\Delta f = f_{\text{exc}} - f_0$ in the frequency-modulated AFM mode for different cases using a Morse potential

$$V_{\text{Morse}} (d) = E_b \left[-2 \exp^{-\kappa(d-\sigma_0)} + \exp^{-2\kappa(d-\sigma_0)} \right] \quad (26)$$

as a model that describes the interaction between two atoms at a distance d by the parameters $E_b = 0.371$ aJ, $\sigma_0 = 0.235$ nm, and $\kappa = 4.25$ nm^{-1} (adapted from [20]). We use this model for the pairwise interaction between a tip with a heterogeneous surface section. The surface section is built by arranging $N_a = 5$ atoms at $z_{\text{ts}} = 0$ nm along the x-axis (with unit vector $\vec{e}_x$) at an atom–atom distance of $d_a = 0.5$ nm. To model a second atomic species for the heterogeneous surface section, E_b of the central atom is scaled by a factor of four. A sixth probe atom at position $\vec{r}_{\text{ts}}$ representing the tip is moved within the force field $\vec{F}_{\text{ts}} (\vec{r}_{\text{ts}})$ calculated from

$$\vec{F}_{\text{ts}} (\vec{r}_{\text{ts}}) = -\nabla \sum_{i=1}^{N_a} V_{\text{Morse}} \left(\left| \vec{r}_{\text{ts}} - \left(\vec{r}_a + i d_a \vec{e}_x \right) \right| \right). \qquad (27)$$

Vector $\vec{r}_a$ defines the origin of the surface section. In the following, the central atom is placed at $\vec{r}_a = (x_{\text{ts}}, y_{\text{ts}}, z_{\text{ts}}) = (0.35, 0, 0)$ nm. The potential V_{Morse} and the force components $F_{\text{ts}}^x = \vec{F}_{\text{ts}} \cdot \vec{e}_x$ as well as $F_{\text{ts}}^z = \vec{F}_{\text{ts}} \cdot \vec{e}_z$ are shown in Figure 3a, b,

and c, respectively. A vectorial representation of the force field in the x_{ts}–z_{ts} plane is included in Figure 3a.
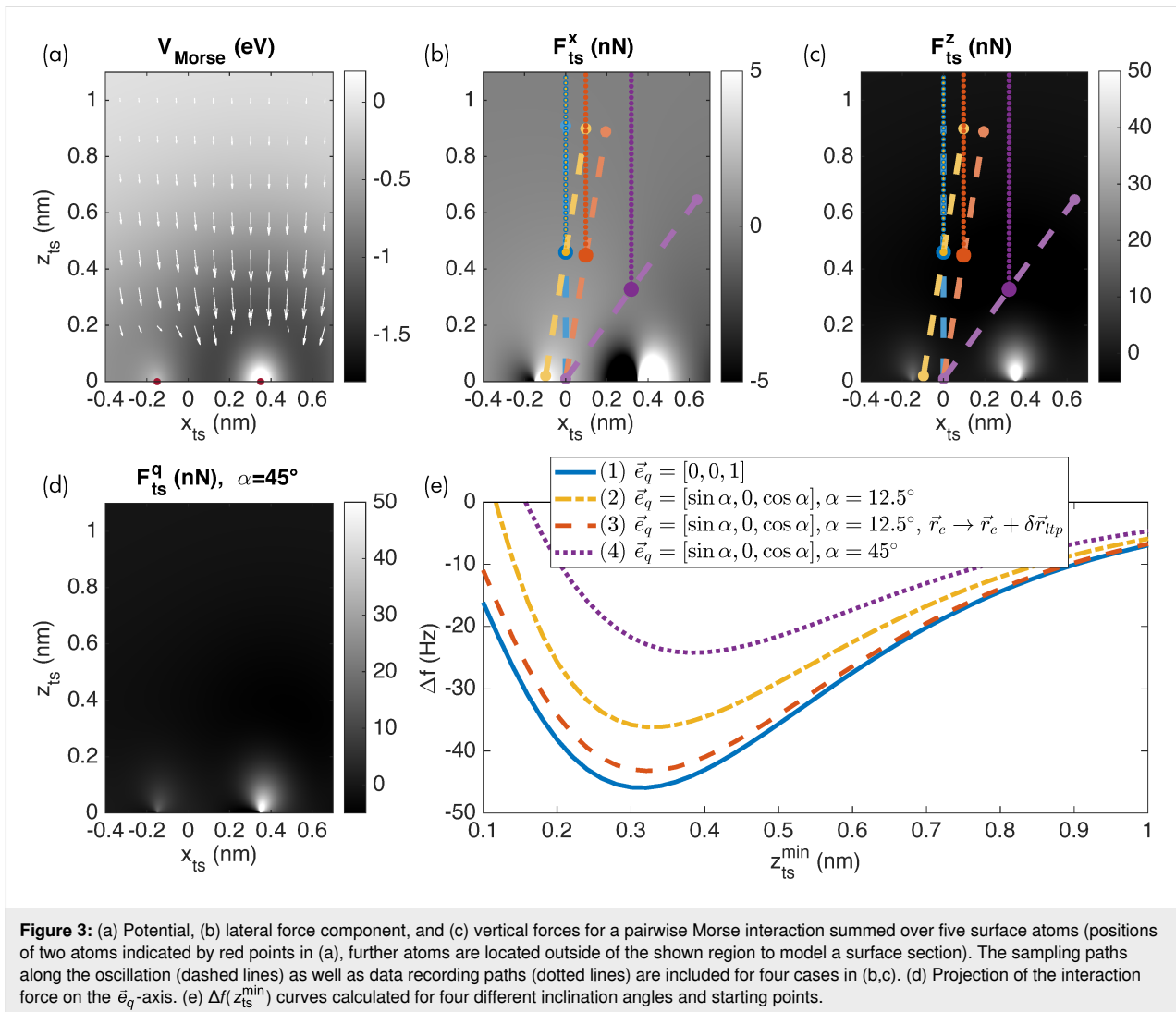
To illustrate the effects resulting from an inclined tip oscillation, four cases are discussed. Common to all cases is that the data recording path, described by the oscillation centre positions $\vec{r}_{\text{c}}$, remains oriented parallel to the $\vec{e}_z$-axis, that is, perpendicular to the surface as indicated by the dotted lines in Figure 3b and Figure 3c. This represents the common experimental protocol. In turn, the sampling path describing the tip oscillation is inclined by different angles α within the x_{ts}–z_{ts} plane with the normalised inclined oscillation vector $\vec{e}_q = [\sin\alpha, 0, \cos\alpha]$. The tip trajectories during single oscillation cycles at one fixed $\vec{r}_{\text{c}}$ are indicated for each case by dashed lines in Figure 3b and Figure 3c.

The force component F_{ts}^q along the tip path is a scalar quantity and shown for $\alpha = 45°$ in Figure 3d. Compared to the vertical component F_{ts}^z (see Figure 3c), the shape at the atom positions is asymmetric and the absolute contrast is diminished as a result of projecting the vectorial force $\vec{F}_{\text{ts}}$ onto $\vec{e}_q$.

The force gradient $k_{\text{ts}}^{\circ q}$ along the tip path and projected to $\vec{e}_q$ is calculated by numerical differentiation along $\vec{e}_q$ of the F_{ts}^q force field. The result is used to calculate frequency shift Δf data from Equation 23 for $\varphi = -\pi/2$. As an example, we use parameters for a sensor often used in low-temperature environments (tuning fork sensor [21] with $f_0 = 30$ kHz, $k_0 = 1800$ N/m, and $A = 0.45$ nm). However, similar effects can be present when using parameters for other sensors as well. Frequency shift Δf data are calculated with the piezo axis located at $x_{\text{ts}} = y_{\text{ts}} = 0$ and moving the tip along z_p for data recording, while data are plotted as a function of $z_{\text{ts}}^{\text{min}}$.

The solid blue curve in Figure 3e represents case (1) of a perpendicular oscillation with $\vec{e}_q = [0,0,1]$. When positioning the tip along the $\vec{e}_z$-axis for data acquisition, this case allows for a reliable determination of the interaction force F_{ts}^z by applying known inversion strategies [2,4,5].

Next, the tip inclination is set to $\alpha = 12.5°$ within the x_{ts}–z_{ts} plane as case (2) shown in yellow in Figure 3b and Figure 3c. The corresponding $\Delta f^{(2)}(z_{\text{ts}}^{\text{min}})$ curve (dash-dotted yellow in Figure 3e) is different from the blue $\Delta f^{(1)}(z_{\text{ts}}^{\text{min}})$ curve. This is expected as the lower turning point moved sideways and the cap averaging is performed along a different path than in case (1). Note that in contrast to case (1), the tip sampling path has no overlapping segments when moving the tip along z_p. In case (3), the lateral movement of the lower turning point is compensated by subtracting the vector $\delta\vec{r}_{\text{ltp}} = [\Delta x, 0, \Delta z]$ with $\Delta x = -A\sin\alpha$ and $\Delta z = A(1 - \cos\alpha)$ from $\vec{r}_{\text{c}}$. The resulting $\Delta f^{(3)}(z_{\text{ts}}^{\text{min}})$ data

Figure 3: (a) Potential, (b) lateral force component, and (c) vertical forces for a pairwise Morse interaction summed over five surface atoms (positions of two atoms indicated by red points in (a), further atoms are located outside of the shown region to model a surface section). The sampling paths along the oscillation (dashed lines) as well as data recording paths (dotted lines) are included for four cases in (b,c). (d) Projection of the interaction force on the $\vec{e}_q$-axis. (e) $\Delta f(z_{ts}^{min})$ curves calculated for four different inclination angles and starting points.

included as a dashed red curve in Figure 3e deviates from all other curves.
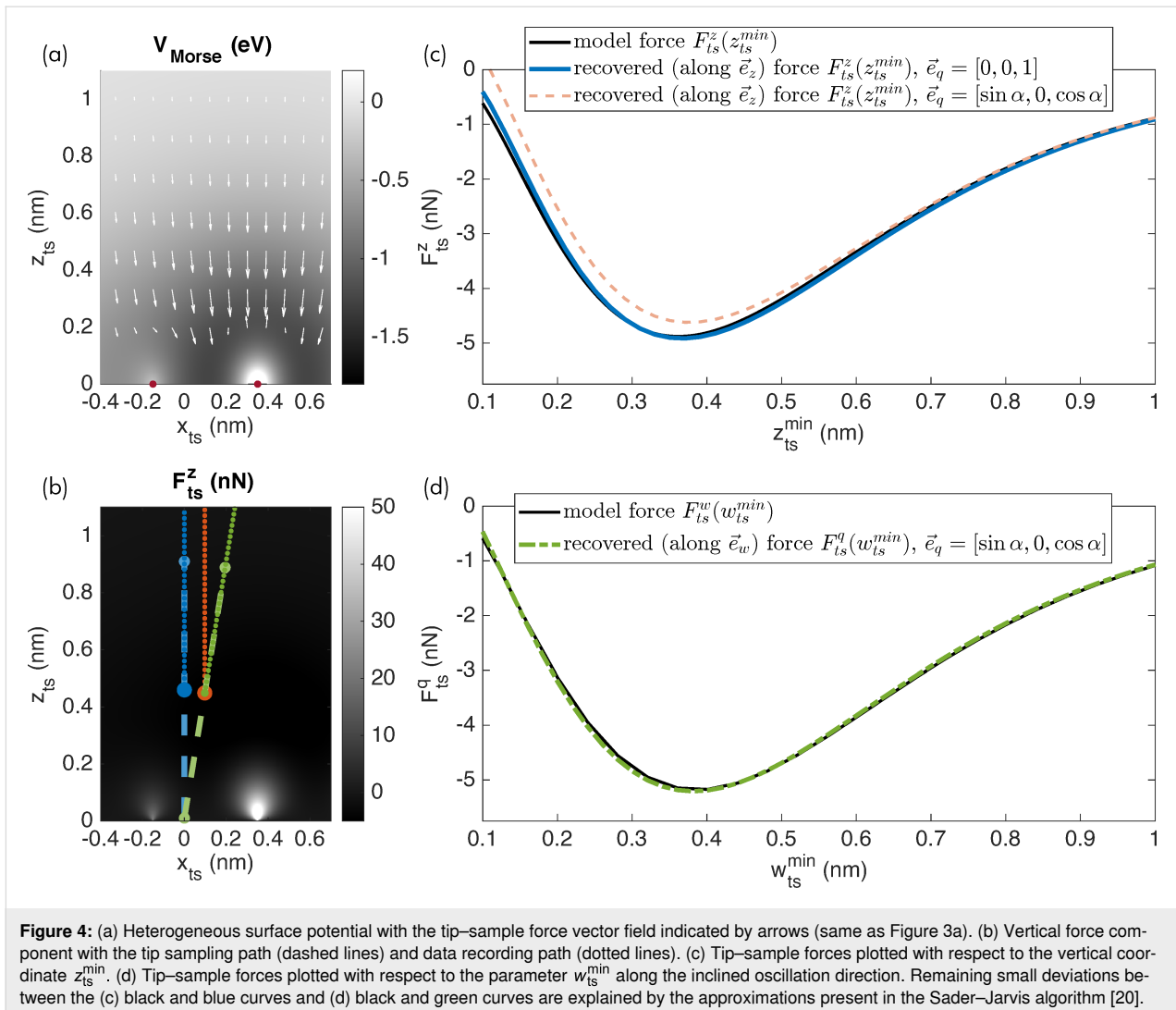
When further increasing the inclination angle α as in case (4), the deviation becomes larger as presented by the violet dotted curve in Figure 3e for α = 45°. Last, we note that lateral components are virtually absent for large tip–sample distances in this model, leading to a convergence of the $\Delta f(z_{ts}^{min})$ curves in the regime $z_{ts}^{min} \gg 1$ nm.

Force deconvolution for the inclined sampling path

The difference in the orientation of $\vec{e}_q$ and $\vec{e}_z$ violates a fundamental assumption of the commonly used inversion algorithms [4,5]: The tip sampling path segments are not overlapping when moving the tip along the data recording path for an inclined oscillation. The resulting error in the force recovery is shown in Figure 4c, where the red dashed curve presents the recovered

force for the case of an oscillation inclined by α = 12.5° and Δf data recorded along $\vec{e}_z$. As is apparent, the force curve does not match the model reference curve, $F_{ts}^z\left(z_{ts}^{min}\right)$, included as the solid black line. In contrast, the force curve recovered for the vertical oscillation and vertical data recording ($\vec{e}_q = [0,0,1]$, blue curve) matches the reference curve.

As a solution to this issue, we propose to orient the recording path for acquiring the AFM observables and parameters parallel to the tip sampling path $\vec{e}_q$ describing the tip oscillation. This modification leads to an overlap of the tip sampling path segments for nearby positions along the data recording path. Therefore, the deconvolution using the known algorithms can be performed in the usual manner. Naturally, the result will not represent the perpendicular force F_{ts}^z, but rather describes the force component F_{ts}^q along the w-axis, parameterised by the scalar variable w_{ts}^{min}. For a conservative force field, the vertical interaction force could in principle be calculated from this result.

Figure 4: (a) Heterogeneous surface potential with the tip–sample force vector field indicated by arrows (same as Figure 3a). (b) Vertical force component with the tip sampling path (dashed lines) and data recording path (dotted lines). (c) Tip–sample forces plotted with respect to the vertical coordinate z_{ts}^{min}. (d) Tip–sample forces plotted with respect to the parameter w_{ts}^{min} along the inclined oscillation direction. Remaining small deviations between the (c) black and blue curves and (d) black and green curves are explained by the approximations present in the Sader–Jarvis algorithm [20].

Additionally, if the full force field is of interest, this can be extracted by systematic measurements of many Δf curves using the appropriate experimental procedures [22].

Simulation results for moving the tip along the inclined path during data acquisition and extracting the force along this path are presented in Figure 4d by the green curve. The force along this data recording path is correctly recovered as shown in Figure 4d where the green dash-dotted curve closely matches the model curve (in solid black) extracted along this path. Note that the force along an inclined w-axis is different from the vertical interaction force along z_{ts}^{min}.

Conclusion

Several conclusions can be drawn from extending the mathematical description of dynamic force microscopy by arbitrary tip sampling and data recording paths. For a typical inclination of $\alpha = 12.5°$, the minimum force was calculated to differ by

more than 5% when compared to a result not taking the inclination into account. The magnitude of this difference depends on the model parameter choice and geometry: The difference can be amplified or reduced depending on the oscillation amplitude, on the interaction potential strength and decay, as well as on the atomic geometry. For example, edges of finite atomic slabs or larger atomic clusters generate significant effects. In practice, a model calculation is required to determine the uncertainty in the measured force due to the inclined tip oscillation.

Precise forces are measured if the data recording path, here introduced as the axis w, is aligned parallel to the tip sampling path, here described as the vector $\vec{e}_q$. The resulting measured force represents the component $F_{ts}^q(w)$ of the tip–sample force along this direction. Despite the formal and quantitative difference from the commonly considered vertical component $F_{ts}^z(z)$, the component along w delivers identical physical insights into the tip–sample interaction.

Appendix: Mathematical Derivations
AFM Equation 1

The first AFM equation follows from evaluating the Fourier coefficient $F_{\text{even}}^{\text{q},0}$, defined by

$$F_{\text{even}}^{\text{q},0} = \left\langle \vec{F}_{\text{ts}} \cdot \vec{e}_q \right\rangle = \left\langle F_{\text{ts}}^q \right\rangle_t. \tag{28}$$

The tip–sample force can furthermore be written as a sum of an even and an odd force

$$= \left\langle \vec{F}_{\text{even}} \cdot \vec{e}_q \right\rangle_t + \left\langle \vec{F}_{\text{odd}} \cdot \vec{e}_q \right\rangle_t. \tag{29}$$

By definition of an odd force, the time average $\left\langle \vec{F}_{\text{odd}} \cdot \vec{e}_q \right\rangle_t$ evaluates to zero. We compare this equation by introducing the equation of motion (Equation 6) for F_{ts}^q and using the fact that the time average is a linear functional

$$= \frac{k_0}{\left(2\pi f_0\right)^2} \left\langle \ddot{q} \right\rangle_t + k_0 \left\langle q \right\rangle_t + \frac{k_0}{2\pi f_0 Q_0} \left\langle \dot{q} \right\rangle_t - \left\langle F_{\text{exc}} \right\rangle_t. \tag{30}$$

With the harmonic approximation (Equation 2) it can directly be shown that $\left\langle \dot{q} \right\rangle_t = \left\langle \ddot{q} \right\rangle_t = \left\langle F_{\text{exc}} \right\rangle_t = 0$ and $q_s = \left\langle q \right\rangle_t$. The first AFM equation directly follows as

$$\left\langle \vec{F}_{\text{even}} \cdot \vec{e}_q \right\rangle_t = k_0 q_s. \tag{31}$$

AFM Equation 2

The Fourier coefficient $F_{\text{even}}^{\text{q},1}$ is defined as

$$F_{\text{even}}^{\text{q},1} = 2 \left\langle \vec{F}_{\text{ts}} \cdot \vec{e}_q \cos\left(2\pi f_{\text{exc}} t + \varphi\right) \right\rangle_t. \tag{32}$$

Within the harmonic approximation (Equation 2), this term can be written as

$$= \frac{2}{A} \left\langle \vec{F}_{\text{ts}} \cdot \vec{e}_q \left(q - q_s\right) \right\rangle_t \tag{33}$$

and $\vec{F}_{\text{ts}}$ be expressed by even and odd forces

$$= \frac{2}{A} \left\langle \vec{F}_{\text{even}} \cdot \vec{e}_q \left(q - q_s\right) \right\rangle_t + \frac{2}{A} \left\langle \vec{F}_{\text{odd}} \cdot \vec{e}_q \left(q - q_s\right) \right\rangle_t \tag{34}$$

whereby the average $\left\langle \vec{F}_{\text{odd}} \cdot \vec{e}_q \left(q - q_s\right) \right\rangle_t$ evaluates to zero. Using the equation of motion (Equation 6), the Fourier coefficient can be written as

$$= \frac{2k_0}{A\left(2\pi f_0\right)^2} \left[\left\langle \ddot{q}q \right\rangle_t - q_s \left\langle \ddot{q} \right\rangle_t \right] + \frac{2k_0}{A} \left[\left\langle q^2 \right\rangle_t - q_s \left\langle q \right\rangle_t \right] + \frac{2k_0}{A 2\pi f_0 Q_0} \left[\left\langle \dot{q}q \right\rangle_t - q_s \left\langle \dot{q} \right\rangle_t \right] - \frac{2}{A} \left[\left\langle F_{\text{exc}} q \right\rangle_t - q_s \left\langle F_{\text{exc}} \right\rangle_t \right]. \tag{35}$$

In full analogy to [3], this equation evaluates to

$$= k_0 A \left(1 - \frac{f_{\text{exc}}^2}{f_0^2}\right) - F_{\text{exc}} \cos\varphi \tag{36}$$

whereby the identities $\left\langle q \right\rangle_t = \left\langle \dot{q} \right\rangle_t = \left\langle \ddot{q} \right\rangle_t = \left\langle \dot{q}q \right\rangle_t = \left\langle F_{\text{exc}} \right\rangle_t = 0$ are used.

AFM Equation 3

The Fourier coefficient $F_{\text{odd}}^{\text{q},1}$ is defined as

$$F_{\text{odd}}^{\text{q},1} = 2 \left\langle \vec{F}_{\text{ts}} \cdot \vec{e}_q \sin\left(2\pi f_{\text{exc}} t + \varphi\right) \right\rangle_t \tag{37}$$

which can be written as

$$= -\frac{2}{2\pi f_{\text{exc}} A} \left\langle \vec{F}_{\text{ts}} \cdot \vec{e}_q \dot{q} \right\rangle_t \tag{38}$$

by using the harmonic approximation, Equation 2. The force is again expressed as a sum of even and odd contributions

$$= -\frac{2}{2\pi f_{\text{exc}} A} \left[\left\langle \vec{F}_{\text{even}} \cdot \vec{e}_q \dot{q} \right\rangle_t + \left\langle \vec{F}_{\text{odd}} \cdot \vec{e}_q \dot{q} \right\rangle_t \right] \tag{39}$$

whereby $\left\langle \vec{F}_{\text{even}} \cdot \vec{e}_q \dot{q} \right\rangle_t$ evaluates to zero. Using the equation of motion, Equation 6, this is equal to

$$= -\frac{2}{2\pi f_{\text{exc}} A} \left[\frac{k_0}{\left(2\pi f_0\right)^2} \left\langle \ddot{q}\dot{q} \right\rangle_t + k_0 \left\langle q\dot{q} \right\rangle_t + \frac{k_0}{2\pi f_0 Q_0} \left\langle \dot{q}^2 \right\rangle_t - \left\langle F_{\text{exc}} \dot{q} \right\rangle_t \right]. \tag{40}$$

With the identities $\left\langle \ddot{q}\dot{q} \right\rangle_t = \left\langle \dot{q}q \right\rangle_t = 0$, this term evaluates to

$$= -\frac{k_0 A}{Q_0} \frac{f_{\text{exc}}}{f_0} - F_{\text{exc}} \sin\varphi. \tag{41}$$

Funding

ORCID® iDs

Philipp Rahe - https://orcid.org/0000-0002-2768-8381
Daniel Heile - https://orcid.org/0000-0002-2315-5633
Reinhard Olbrich - https://orcid.org/0000-0001-7765-393X
Michael Reichling - https://orcid.org/0000-0003-3186-9000

References

1. Gross, L.; Schuler, B.; Pavliček, N.; Fatayer, S.; Majzik, Z.; Moll, N.; Peña, D.; Meyer, G. *Angew. Chem., Int. Ed.* **2018,** *57,* 3888–3908. doi:10.1002/anie.201703509
2. Heile, D.; Olbrich, R.; Reichling, M.; Rahe, P. *Phys. Rev. B* **2021,** *103,* 075409. doi:10.1103/physrevb.103.075409
3. Söngen, H.; Bechstein, R.; Kühnle, A. *J. Phys.: Condens. Matter* **2017,** *29,* 274001. doi:10.1088/1361-648x/aa6f8b
4. Sader, J. E.; Jarvis, S. P. *Appl. Phys. Lett.* **2004,** *84,* 1801–1803. doi:10.1063/1.1667267
5. Giessibl, F. J. *Appl. Phys. Lett.* **2001,** *78,* 123–125. doi:10.1063/1.1335546
6. Heim, L.-O.; Kappl, M.; Butt, H.-J. *Langmuir* **2004,** *20,* 2760–2764. doi:10.1021/la036128m
7. Hutter, J. L. *Langmuir* **2005,** *21,* 2630–2632. doi:10.1021/la047670t
8. Gates, R. S. *Rev. Sci. Instrum.* **2017,** *88,* 123710. doi:10.1063/1.4986201
9. Edwards, S. A.; Ducker, W. A.; Sader, J. E. *J. Appl. Phys.* **2008,** *103,* 064513. doi:10.1063/1.2885734
10. Wang, F. *J. Appl. Phys.* **2009,** *106,* 096103. doi:10.1063/1.3257268
11. Cannara, R. J.; Brukman, M. J.; Carpick, R. W. *Rev. Sci. Instrum.* **2005,** *76,* 053706. doi:10.1063/1.1896624
12. Wang, C.; Sun, J.; Itoh, H.; Shen, D.; Hu, J. *Anal. Sci.* **2011,** *27,* 143–147. doi:10.2116/analsci.27.143
13. Misaka, T.; Kajimoto, K.; Araki, K.; Otsuka, Y.; Matsumoto, T. *Jpn. J. Appl. Phys.* **2020,** *59,* 090906. doi:10.35848/1347-4065/abac6e
14. Garrett, J. L.; Krayer, L. J.; Palm, K. J.; Munday, J. N. *Appl. Phys. Lett.* **2017,** *111,* 043105. doi:10.1063/1.4996720
15. D'Amato, M. J.; Marcus, M. S.; Eriksson, M. A.; Carpick, R. W. *Appl. Phys. Lett.* **2004,** *85,* 4738–4740. doi:10.1063/1.1812839
16. Marcus, M. S.; Carpick, R. W.; Sasaki, D. Y.; Eriksson, M. A. *Phys. Rev. Lett.* **2002,** *88,* 226103. doi:10.1103/physrevlett.88.226103
17. Gretz, O.; Weymouth, A. J.; Holzmann, T.; Pürckhauer, K.; Giessibl, F. J. *Beilstein J. Nanotechnol.* **2021,** *12,* 517–524. doi:10.3762/bjnano.12.42
18. Lübbe, J.; Doering, L.; Reichling, M. *Meas. Sci. Technol.* **2012,** *23,* 045401. doi:10.1088/0957-0233/23/4/045401
19. Albrecht, T. R.; Grütter, P.; Horne, D.; Rugar, D. *J. Appl. Phys.* **1991,** *69,* 668–673. doi:10.1063/1.347347
20. Welker, J.; Illek, E.; Giessibl, F. J. *Beilstein J. Nanotechnol.* **2012,** *3,* 238–248. doi:10.3762/bjnano.3.27
21. Falter, J.; Stiefermann, M.; Langewisch, G.; Schurig, P.; Hölscher, H.; Fuchs, H.; Schirmeisen, A. *Beilstein J. Nanotechnol.* **2014,** *5,* 507–516. doi:10.3762/bjnano.5.59
22. Rahe, P.; Schütte, J.; Schniederberend, W.; Reichling, M.; Abe, M.; Sugimoto, Y.; Kühnle, A. *Rev. Sci. Instrum.* **2011,** *82,* 063704. doi:10.1063/1.3600453

License and Terms